STEM CELLS®

TRANSLATIONAL AND CLINICAL RESEARCH

Mesenchymal Stem Cells Enhance Wound Healing Through Differentiation and Angiogenesis

YAOJIONG WU, LIWEN CHEN, PAUL G. SCOTT, EDWARD E. TREDGET

Department of Surgery, University of Alberta, Edmonton, Alberta, Canada

Key Words. Angiogenesis • Regeneration/repair • Diabetic mice • Vascular endothelial growth factor • Ang-1

ABSTRACT

Although chronic wounds are common, treatment for these disabling conditions remains limited and largely ineffective. In this study, we examined the benefit of bone marrow-derived mesenchymal stem cells (BM-MSCs) in wound healing. Using an excisional wound splinting model, we showed that injection around the wound and application to the wound bed of green fluorescence protein $(GFP)^+$ allogeneic BM-MSCs significantly enhanced wound healing in normal and diabetic mice compared with that of allogeneic neonatal dermal fibroblasts or vehicle control medium. Fluorescence-activated cell sorting analysis of cells derived from the wound for GFP-expressing BM-MSCs indicated engraftments of 27% at 7 days, 7.6% at 14 days, and 2.5% at 28 days of total BM-MSCs administered. BM-MSC-treated wounds exhibited significantly accelerated wound closure, with increased re-epithelialization, cellularity, and angiogenesis. Notably, BM-MSCs, but not $CD34^+$ bone marrow cells in the wound, expressed the keratinocyte-specific protein keratin and formed glandular structures, suggesting a direct contribution of BM-MSCs to cutaneous regeneration. Moreover, BM-MSC-conditioned medium promoted endothelial cell tube formation. Real-time polymerase chain reaction and Western blot analysis revealed high levels of vascular endothelial growth factor and angiopoietin-1 in BM-MSCs and significantly greater amounts of the proteins in BM-MSC-treated wounds. Thus, our data suggest that BM-MSCs promote wound healing through differentiation and release of proangiogenic factors. STEM CELLS *2007;25:2648–2659*

Disclosure of potential conflicts of interest is found at the end of this article.

INTRODUCTION

Optimum healing of a cutaneous wound requires a well-orchestrated integration of the complex biological and molecular events of cell migration and proliferation and extracellular matrix (ECM) deposition, angiogenesis, and remodeling [1–3]. However, this orderly progression of the healing process is impaired in many chronic diseases, including diabetes [2]. Of the 150 million people with diabetes worldwide, 15% present suffer from foot ulcerations, which often become nonhealing chronic wounds [4]. Over the past decades, little improvement has been shown in preventing morbidity and disability from chronic wounds [4]. The best available treatment for chronic wounds achieves only a 50% healing rate that is often temporary. Among the many factors contributing to nonhealing wounds, impairment in the production of cytokines by local inflammatory cells and fibroblasts and reduced angiogenesis are crucial [2].

Bone marrow-derived mesenchymal stem cells (BM-MSCs), which are also referred to as stromal progenitor cells, are self-renewing and expandable stem cells. BM-MSCs are able to differentiate into adipocytes, osteoblasts, and chondrocytes [5]. They have also been detected to express phenotypic genes of hepatocytes [6], cardiomyocytes [7], astrocytes, and neurons [8, 9]. Implantation of ex vivo-expanded allogeneic BM-MSCs into swine ischemic myocardium after myocardial infarction led to long-term engraftment, expression of muscle-specific proteins, attenuated contractile dysfunction, and reduced pathologic scarring of the infarcted left ventricular wall [10]. Intracerebral transplantation of BM-MSCs into acid sphingomyelinase-deficient mice was shown to delay the onset of neurological abnormalities and extend their survival [11]. Intravenous infusion of BM-MSCs after stroke in rats reduced the size of infarcts in the brain, with a reduced number of glial cells and enhanced axonal growth in the lesion [12]. Allogeneic BM-MSCs derived from healthy donors have been used to treat diseases in humans [13]; however, their contribution to wound healing has not been fully understood.

In this study, we examined the benefit of BM-MSCs in wound healing on an excisional wound splinting model. We implanted green fluorescence protein (GFP)-expressing allogeneic BM-MSCs into excisional wounds in nondiabetic and diabetic mice and examined their effect on wound healing compared with allogeneic neonatal dermal fibroblasts or vehicle control medium. We assessed wound healing using parameters of re-epithelialization, cellularity, angiogenesis, and dermal structural regeneration. Finally, we examined angiogenic factors in BM-MSCs and BM-MSC-treated wounds compared with vehicle medium- or fibroblast-treated wounds to determine the paracrine effect of BM-MSC-mediated wound healing.

MATERIALS AND METHODS

All animal procedures were approved under the guidelines of the Health Sciences Animal Policy and Welfare Committee of the University of Alberta.

Correspondence: Yaojiong Wu, M.D., Ph.D., 161 HMRC, University of Alberta, 113 Street & 87 Avenue, Edmonton, Alberta T6G 2E1, Canada. Telephone: 780-492-8603; Fax: 780-492-6361; e-mail: yaojiong@ualberta.ca or yjwu2005@yahoo.com; Edward E. Tredget, M.D., M.Sc., FRCSC, Department of Surgery, 2D3.81, 8440 112 Street, University of Alberta, Edmonton, Alberta T6G 2B7, Canada. Telephone: 780-407-6979; Fax: 780-407-7394; e-mail: etredget@gpu.srv.ualberta.ca Received May 28, 2007; accepted for publication June 19, 2007; first published online in STEM CELLS *EXPRESS* July 5, 2007. 1066-5099/2007/$30.00/0 doi: 10.1634/stemcells.2007-0226

Isolation and Purification of MSCs

Bone marrow was collected from the femurs of 5–7-week-old male C57BL/6 or C57-GFP transgenic (C57BL/6 TgN[ACT6EGFP]) mice (Jackson Laboratory, Bar Harbor, ME, http://www.jax.org). The mononuclear fraction of the bone marrow was isolated with a Ficoll-paque density gradient. The nucleated cells were plated in plastic tissue culture dishes and incubated in minimal essential medium (α-MEM; Gibco, Grand Island, NY, http://www.invitrogen.com) supplemented with 17% fetal bovine serum (FBS). BM-MSCs were first selected by their adherent property preferentially attaching to uncoated polystyrene tissue culture dishes [14] and further purified by immunodepletion using magnetic microbeads (Miltenyi Biotec, Bergisch Gladbach, Germany, http://www.miltenyibiotec.com) and monoclonal antibodies against CD34, CD14, Gr1, CD3, and CD19. Passage 3–5 cells were used for the experiments.

Flow Cytometry

Passage 3 BM-MSCs were resuspended in phosphate-buffered saline (PBS) containing 1% bovine serum albumin at 10^6 cells per milliliter. Cell aliquots (100 μl) were first blocked with Mouse BD Fc Block and then incubated with fluorescein isothiocyanate (FITC)- or phycoerythrin-conjugated monoclonal antibodies specific for Sca-1, CD105 (endoglin), CD29, CD44, CD90, CD45, CD14, CD3, CD19, and CD34 or control isotype IgG on ice for 30 minutes. All antibodies were purchased from BD Pharmingen (San Diego, http://www.bdbiosciences.com/pharmingen). For detection of GFP^+ cells in the wounded skin, excised wounds together with a small amount of surrounding skin were dispersed into single-cell suspensions as previously described [15]. In brief, the tissue was incubated with dispase I (Sigma-Aldrich, St. Louis, http://www.sigmaaldrich.com) at 1 mg/ml overnight at 4°C, minced, and incubated in a digestion buffer containing hyaluronidase (1 mg/ml), collagenase D (1 mg/ml), and DNase (150 units/ml) in a 37°C shaking water bath for 2 hours. The dispase and the hyaluronidase digests were pooled and filtered through a 70-μm nylon cell strainer. Cells were pelleted and resuspended in PBS containing 3% FBS and analyzed for GFP-positive cells. Cells from sham wounds were used as negative controls. Ten thousand events were analyzed by flow cytometry (Becton, Dickinson and Company, Franklin Lakes, NJ, http://www.bd.com) using CellQuest software.

MSC Differentiation Assays

Passage 4 BM-MSCs were incubated to differentiate into adipocytes, osteoblasts, and chondrocytes in corresponding induction medium for 3 weeks [5, 14]. Adipogenic medium contained 10^{-6} M dexamethasone, 10 μg/ml insulin, and 100 μg/ml 3-isobutyl-L-methylxantine (Sigma-Aldrich). Osteogenic medium contained 10^{-7} M dexamethasone, 50 μg/ml ascorbic acid, and 10 mM β-glycerophosphate (Sigma-Aldrich). Cultures were stained for alkaline phosphatase (alkaline phosphatase detection kit; Sigma-Aldrich). For chondrocyte differentiation, MSC pellets were cultured in Dulbecco's modified Eagle's medium (high-glucose) containing 10^{-7} M dexamethasone, 50 μg/ml ascorbate-2-phosphate, 100 μg/ml pyruvate (Sigma-Aldrich), 10 ng/ml transforming growth factor-β1 (R&D Systems Inc., Minneapolis, http://www.rndsystems.com), and 50 mg/ml ITS + Premix (6.25 μg/ml insulin, 6.25 μg/ml transferrin, 6.25 ng/ml selenious acid, 1.25 mg/ml bovine serum albumin, and 5.35 mg/ml linoleic acid; BD Biosciences, San Diego, http://www.bdbiosciences.com). The cultures were fixed, sectioned, and stained for Alcian Blue (Sigma-Aldrich) or subjected to RNA extraction and reverse transcription-polymerase chain reaction (RT-PCR) analysis for expression of genes characteristic of chondrocytes [16]. For differentiation of BM-MSCs into keratinocytes, human primary keratinocytes were cultured on two-well chamber slides to 80% confluence in K-SFM (a serum-free medium for keratinocyte culture; Gibco) and then irradiated with 10 Gy from a ^{60}Co source at a dose rate of 0.3 Gy/minute to stop cell proliferation [17]. Twenty-four hours later, 10^4 GFP^+ BM-MSCs were seeded on the keratinocyte monolayer and maintained in K-SFM supplemented with 1% FBS for 1 week. Medium was changed at day 3. Cells were fixed, immunostained with an antibody reacting to cytokeratins (in molecular sizes of 58, 56, 52, 60, 51, and 48 kDa; DAKO, Glostrup, Denmark, http://www.dako.com), and visualized under confocal microscope.

Wound Healing Model and BM-MSC Transplantation

BALB/c mice (8 weeks old; female; body weight, 20–23 g), *db/db* mice (BKS.Cg-*m* +/+ *Lepr^{db}*/J, *db$^+$/db$^+$*; 13 weeks old; female; body weight, 46.3 ± 3.3 g; blood glucose, 44.0 ± 7.7 mM; triglyceride, 1.4 ± 0.6 mM; and cholesterol, 2.4 ± 0.6 mM) and their normal littermates (*db$^+$/m$^+$*; 13 weeks old; female; body weight, 22.4 ± 1.6 g; blood glucose, 12.6 ± 10.8 mM; triglyceride, 0.8 ± 0.2 mM; and cholesterol, 1.5 ± 0.2 mM; *t* test, $p < .01$) were obtained from Jackson Laboratory. The animals were randomly divided into three groups, and the excisional wound splinting model was generated as described previously [18]. In brief, after hair removal from the dorsal surface and anesthesia, two 6-mm full-thickness excisional skin wounds were created on each side of the midline. Each wound received 1 million cells (GFP^+ BM-MSCs or neonatal dermal fibroblasts derived from C57BL/6 or C57BL/6-GFP mice): 0.7×10^6 in 60 μl of PBS injected intradermally around the wound at four injection sites and 0.3×10^6 in 20 μl of growth factor-reduced Matrigel (BD Biosciences) applied onto the wound bed. In some experiments, equal numbers of $CD34^+$ murine bone marrow cells isolated with antibody-coated magnetic microbeads (Miltenyi Biotec) were implanted into excisional wounds in athymic nude mice (8 weeks old; female; Jackson Laboratory). A donut-shaped silicone splint was placed so that the wound was centered within the splint. An immediate-bonding adhesive (Krazy Glue, Columbus, OH, http://www.krazyglue.com) was used to fix the splint to the skin, followed by interrupted sutures to stabilize its position (Fig. 1A), and Tegaderm (3M, London, ON, Canada, http://www.3m.com) was placed over the wounds. The animals were housed individually. We tested the adhesive on the skin in mice prior to this experiment and did not observe any skin irritation or allergic reaction.

Wound Analysis

Digital photographs of wounds were taken at days 0, 3, 7, 10, 14, 21, and 28. Time to wound closure was defined as the time at which the wound bed was completely re-epithelialized and filled with new tissue. Wound area was measured by tracing the wound margin and calculated using an image analysis program (NIH Image). The investigators measuring samples were blinded to group and treatment. The percentage of wound closure was calculated as follows: (Area of original wound − Area of actual wound)/Area of original wound × 100. The inside edge of the splint exactly matched the edge of the wound, so that the splinted hole was used to represent the original wound size. Mice were sacrificed at 7, 14, and 28 days, at which times, skin samples including the wound and 4 mm of the surrounding skin were harvested using a 10-mm biopsy punch. For whole skin mount, the entire wound and surrounding skin was placed on plastic (tissue culture dish) with the dermis side down and photographed immediately.

Histologic Examination

Tissue specimens were fixed in 3% paraformaldehyde for 24 hours and embedded in OCT. Six-micron-thick sections were stained with H&E for light microscopy. Histological scoring was performed in a blinded fashion. Each slide was given a histological score ranging from 1 to 10 according to the following parameters, modified from previous reports [19, 20]: re-epithelialization and regeneration, dermal cellularity, granulation tissue formation, and angiogenesis. Capillary density was assessed morphometrically by examining three fields per section of the wound between the edges in six successive sections after immunofluorescence staining for endothelial cells with an anti-CD31 antibody [21, 22]. The criteria used for histological scores of wound healing are summarized in Table 1.

For immunofluorescence, tissue sections were preincubated with sodium borohydride (1 mg/ml in PBS) to reduce autofluorescence. Endogenous biotin was blocked with streptavidin biotin

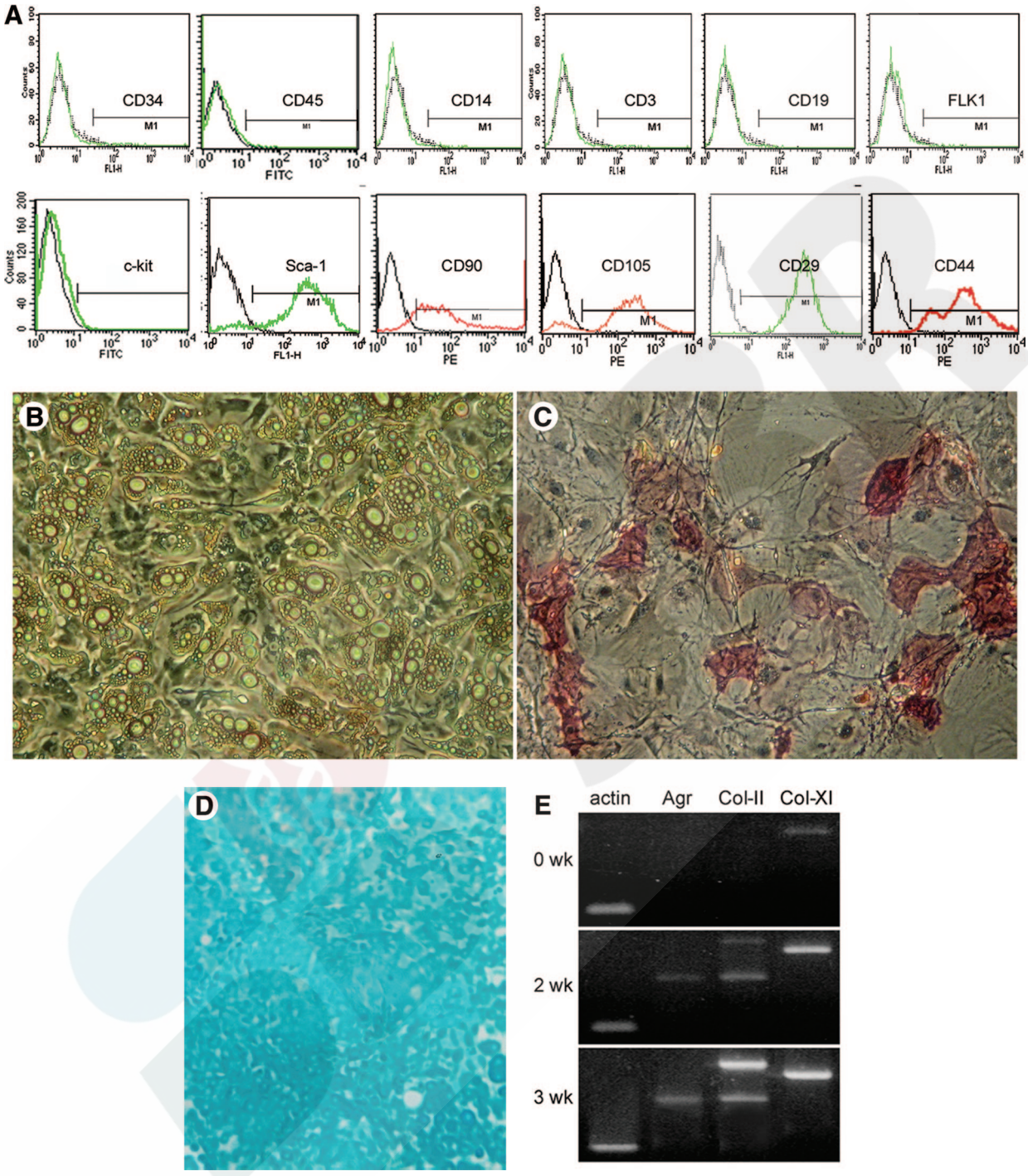

Figure 1. Characterization of BM-MSCs. **(A):** Fluorescence-activated cell sorting (FACS) analysis of BM-MSCs. Passage 3 BM-MSCs were analyzed by FACS after staining with FITC- or PE-conjugated control isotype IgG (gray peaks) or antibodies against indicated cell surface proteins. **(B):** Differentiation of BM-MSCs. Cultured in appropriate differentiation media, BM-MSCs differentiated into adipocytes, which are indicated by accumulation of lipid vesicles in the cells **(B)**, osteoblasts, which expressed alkaline phosphatase, as indicated in red **(C)**, and chondrocytes in pellet culture, which were positive for proteoglycans, as indicated in blue after Alcian Blue stain **(D)** and expressed genes characteristic of chondrocytes by reverse transcription-polymerase chain reaction **(E)**. Primers for Col-II detected procollagen IIa (upper band) and IIb transcripts. Abbreviations: Actin, β-actin; Agr, aggrecan; Col, collagen; Col-II, procollagen II; FITC, fluorescein isothiocyanate; PE, phycoerythrin; wk, week(s).

blocking kit (Vector Laboratories, Burlingame, CA, http://www.vectorlabs.com). Keratinocytes were stained with an antibody against epidermal keratin subunits (DAKO). GFP was detected with an antibody (USBiological, Swampscott, MA, http://www.usbio.net) and visualized with a FITC-conjugated secondary antibody. Endothelial cells were identified with an antibody against CD31 or von Willebrand factor (vWF; BD Biosciences) followed by incubation with a biotinylated secondary antibody (Jackson ImmunoResearch, West Grove, PA, http://www.jacksonimmuno.com) and visualized with Fluor 568-conjugated streptavidin (Invitrogen, Carlsbad, CA, http://www.invitrogen.com). Nuclear staining with Hoechst and Ki67 (DAKO) was performed as previously described [23]. Isotype control antibodies were used for negative controls. Sections were examined with a Zeiss LSM 510 confocal microscope

Table 1. Criteria for histological scores

Score	Epidermal and dermal regeneration	Cell infiltration	Granulation tissue	Angiogenesis (day 14 wounds only)
1–3	Minimal to moderate re-epithelialization with or without minimal developing glandular structure formation in the wound	Wound covered with thin to moderate cell layer	Granulation around wound edges only	Capillary density $<400/mm^2$
4–7	Complete re-epithelialization with minimal developing glandular structure formation in the wound	Wound covered with thick cell layer	Granulation around wound edge and in 30%–50% of wound bed	Capillary density $400–600/mm^2$
8–10	Complete re-epithelialization with considerable developing glandular structure formation in the wound	Wound covered with very thick and densely populated cell layer	Thick granulation around wound edge and in >50% of wound bed	Capillary density $>600/mm^2$

(Carl Zeiss, Jena, Germany, http://www.zeiss.com). The percentages of Ki67-positive nuclei were determined by counting Ki67-positive nuclei and total nuclei in five random fields per section between wound edges using an image analysis program (NIH Image), and four successive sections per wound were analyzed. Appendage-like structures in each wound section between wound edges were photographed to determine the numbers of total appendage-like structures and Ki67-positive appendage-like structures (with more than 10% Ki67-postive nuclei) per section.

X and Y Chromosome Fluorescence In Situ Hybridization

X and Y chromosome fluorescence in situ hybridization (FISH) was performed as previously described with minor modification [6]. In brief, tissue sections 6 μm in thickness were fixed three times in Carnoy fixative and then incubated with an anti-pan-cytokeratin antibody (DAKO). Sections were digested with proteinase K (10 μg/ml; Sigma-Aldrich) and denatured at 72°C for 5 minutes in preheated 70% formamide in 2× standard saline citrate buffer (pH 7.0). After dehydration, a mixture of FITC-labeled mouse X-chromosome probe and Cy3-labeled Y-chromosome probe (STAR FISH; Cambio, Dry Drayton, U.K., http://www.cambio.co.uk) were incubated with tissue sections overnight at 42°C. Sections were incubated with the anti-pan-cytokeratin antibody again followed by staining with a Cy5-conjugated secondary antibody. Nuclei were stained with Hoechst. Sections were examined with a confocal microscope.

Endothelial Cell Network Formation Assay

Human umbilical vein endothelial cells (HUVECs) (2.5×10^4 cells per well) were suspended in 0.4 ml of epithelial growth medium (EGM)-2 basal medium supplemented with 2% FBS and a EGM-2 SingleQuot kit (Cambrex, Walkersville, MD, http://www.cambrex.com), vehicle-, fibroblast-, or BM-MSC-conditioned EGM-2 basal medium supplemented with 0.75% FBS alone; seeded onto Matrigel (BD Biosciences)-coated 24-well plates; and incubated at 37°C/5% CO_2 for 12 hours. After removal of the medium, the cells were fixed, and images were captured. The total length of the tube-like structures was determined using NIH Image software [24]. Four random fields were measured for each well.

Real-Time PCR Analysis

Total RNA was extracted (RNeasy Mini Kit; Qiagen, Hilden, Germany, http://www1.qiagen.com) from cultured BM-MSCs or neonatal dermal fibroblasts that were 80% confluent and had been treated in hypoxic conditions (<1% O_2) for 8 hours and reverse transcribed using the SuperScript First-Strand Synthesis kit (Invitrogen). The primers are as follows: vascular endothelial growth factor (VEGF)-α, forward 5'-AGAGCAACATCACCATGCAG-3', reverse 5'-CAGTGAACGCTCCAGGATTT-3'; angiopoietin (Ang)-2, forward 5'-GACTTCCAGAGGACGTGGAAAG-3', reverse 5'-CTCATTGCCCAGCCAGTACTC-3'; Ang-1, forward 5'-TTGTGATTCTGGTGATTGTGG-3', reverse 5'-CTTGTTTCGCTTTATTTTTGT-3'; and glyceraldehyde-3-phosphate dehydrogenase (GAPDH), forward 5'-ATCATCCCTGCATCCACT-3', reverse 5'-ATCCACGACGGACACATT-3'. Reactions were performed using SYBR Green PCR master mix (Applied Biosystems, Foster City, CA, http://www.appliedbiosystems.com) in a Bio-Rad iCycler iQ Detection System (Hercules, CA, http://www.bio-rad.com). As an internal control, levels of GAPDH were quantified in parallel with target genes. Normalization and fold changes were calculated using the $\Delta\Delta$Ct method [25].

Western Blotting

Western blots were performed as previously described [26]. Briefly, tissue proteins were extracted in a lysis buffer containing 1% Triton X-100 and proteinase inhibitors (Sigma-Aldrich). Equal amounts of total protein (100 μg for lysates and 25 μg for conditioned media) were separated on 12% SDS-polyacrylamide gel electrophoresis gels by electrophoresis and transferred to nitrocellulose membranes. Membranes were incubated overnight at 4°C with monoclonal antibody against Ang-1, Ang-2 (Chemicon, Temecula, CA, http://www.chemicon.com), or VEGF-α (R&D Systems).

Statistical Analysis

All values are expressed as mean ± SD. Student's paired t test was performed for comparison of data of paired samples, and analysis of variance was used for multiple group comparisons, followed by Friedman's post test. A probability (p) value <.05 was considered significant.

RESULTS

Characterization of BM-MSCs

Fluorescence-activated cell sorting (FACS) analysis of our BM-MSCs showed that they were negative for lineage cell markers such as CD34, CD45, CD14, CD3, and CD19 and strongly expressed typical surface antigens such as Sca-1, CD29, CD44, CD105, and CD90 (Fig. 1A). When cultured in adipogenic, osteogenic, or chondrogenic medium, they differentiated into adipocytes (Fig. 1B), osteoblasts (Fig. 1C), or chondrocytes (Fig. 1D, 1E).

BM-MSCs Enhance Wound Healing

BM-MSC-treated wounds exhibited accelerated wound closure in BALB/c mice (Fig. 2A, 2B) and genetically diabetic *db/db* mice (Fig. 2C) compared with fibroblast- or vehicle medium-treated wounds. The enhancement appeared early, at 3 days after implantation in BALB/c mice, and became more evident after 7 days in both BALB/c and *db/db* mice. At 7 days, wound closure in BM-MSC-treated *db/db* mice appeared similar to that in *db/m* mice. At 28 days, 4 of 12 wounds in BM-MSC-treated *db/db* mice ($n = 6$) achieved complete wound closure, but no completely closed wounds were seen in fibroblast-treated ($n = 6$) or vehicle medium-treated ($n = 5$) mice. As splints in some *db/m*

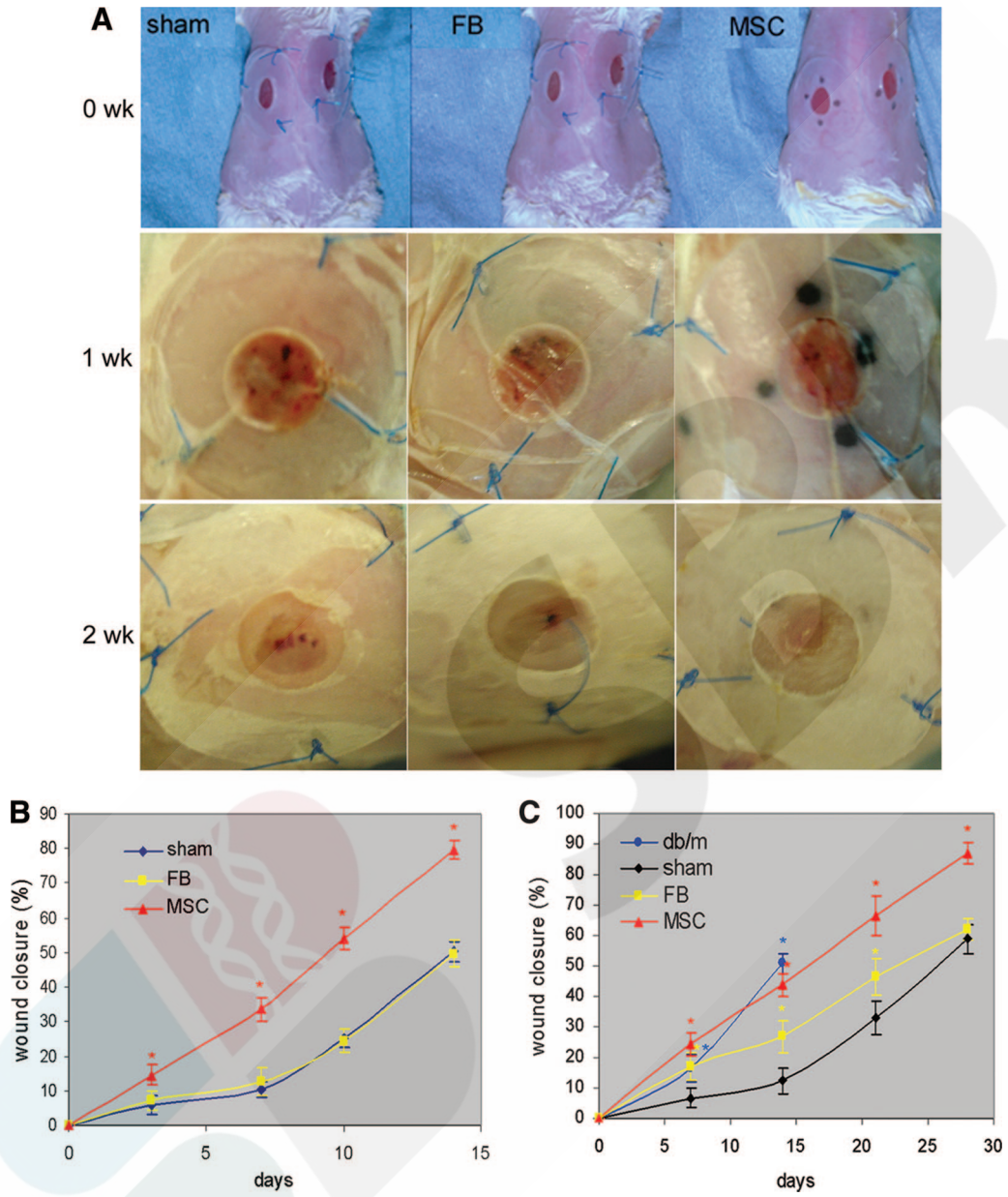

Figure 2. Effects of MSC on wound closure. **(A):** Images of wounds in BALB/c mice. Murine excisional wound splinting model (top panel), in which wounds received implantation of GFP^+ MSC, FB, or control vehicle medium (sham). Representative photographs of the wounds at day 7 (with transparent Tegaderm dressing, middle panel) and day 14 (after removal of dressing, bottom panel). **(B):** Wound measurement of sham group (n = 11 at days 3 and 7; n = 6 at days 10 and 14), FB group (n = 12 at days 3 and 7; n = 7 at days 10 and 14), and MSC group (equal animal numbers to FB group) in BALB/c mice. Analysis of variance (ANOVA), versus sham or FB, *, $p < .001$. **(C):** Wound measurement of sham group in *db/m* mice at days 3 and 7 (n = 10), sham group (n = 6 at days 7 and 14; n = 5 at days 21 and 28), FB group (n = 7 at days 7 and 14; n = 6 at days 21 and 28) and MSC group (equal animal numbers to FB group) in *db/db* mice. ANOVA, *, $p < .01$. Abbreviations: FB, fibroblasts; MSC, bone marrow-derived MSCs; wk, week(s).

mice were not tightly adherent to the skin and failed to restrict skin contraction after 14 days because of movement and hair regrowth, data on wound closure in these mice after 14 days were excluded. In contrast, splints remained firmly adherent to the skin in *db/db* mice, as the animals had slower physical movement and hair regrowth. Fibroblast-treatment accelerated wound closure in *db/db* mice at 7, 14, and 21 days ($p < .01$) but not at 28 days and in BALB/c mice compared with vehicle medium treatment.

Histological evaluation of wounds in BALB/c mice at 7 days disclosed enhanced re-epithelialization in BM-MSC-treated wounds (complete epithelialization in all 10 wounds examined; n = 5) compared with fibroblast-treated wounds (complete re-epithelialization in 6 of 10 wounds; n = 5) or vehicle medium-treated wounds (complete re-epithelialization in 4 of 10 wounds; n = 5). Analysis of day 7 and 14 wounds indicated that BM-MSC-treated wounds had enhanced cellularity (Fig. 3A, 3B) and increased vasculature (also shown in Fig. 5). In addition, granulation tissue in BM-MSC-treated wounds appeared to be thicker and larger. Consistent with these findings, the histological scores of BM-MSC-treated wounds of 7 and 14 days were significantly higher (Fig. 3C; n = 5; $p <$ .001). In addition, BM-MSC-treated wounds appeared to have increased numbers of skin appendages (Fig. 3A), suggesting

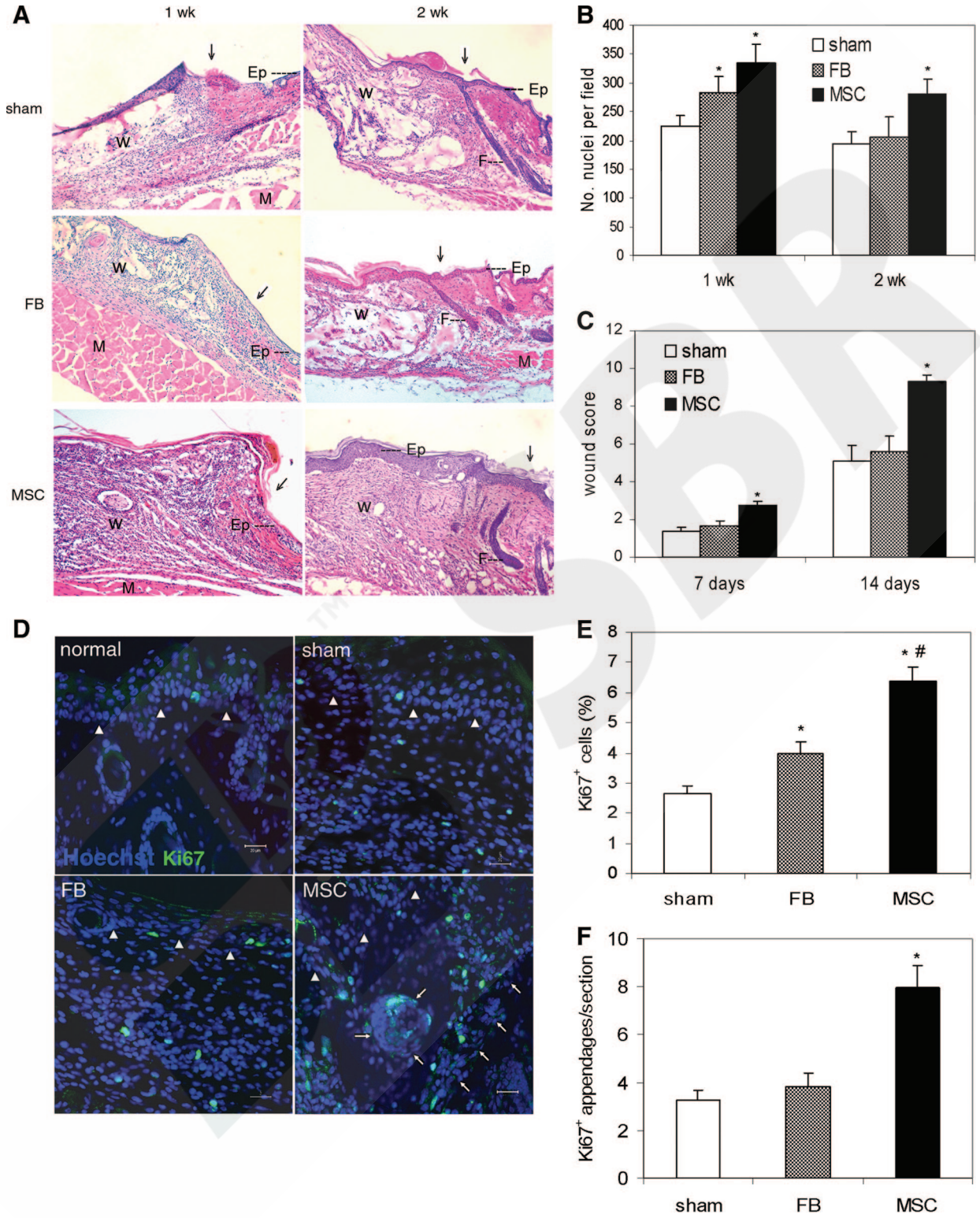

Figure 3. Histological analysis of wounds in BALB/c mice. **(A):** Wound histological images (H&E stain). Wound edges are indicated by arrows. **(B):** Wound cellularity was determined by counting the number of nuclei per high-power (×400) field ($n = 5$; ∗, $p < .01$). **(C):** Wound histological scores ($n = 5$ at days 7 and 14; analysis of variance [ANOVA], ∗, $p < .001$). **(D):** Confocal images show Ki67 and Hoechst stain of normal skin or day 7 wounds treated with vehicle medium (sham), FB, and MSC. Ki67-positive skin appendages are indicated by arrows. The epidermis or wound surfaces are indicated by arrowheads. Scale bar = 20 μm. **(E):** Percentages of Ki67-positive cells in day 7 wounds were counted after immunostaining ($n = 5$; ANOVA, ∗, $p < .01$ MSC or FB vs. sham; #, $p < .001$ MSC vs. FB). **(F):** Numbers of Ki67-positive skin appendages per wound section between wound edges in day 7 wounds ($n = 5$; ∗, $p < .001$ vs. sham or FB). Abbreviations: Ep, epidermis; F, hair follicle; FB, fibroblasts; M, muscle; MSC, bone marrow-derived MSCs; W, wound bed; wk, week(s).

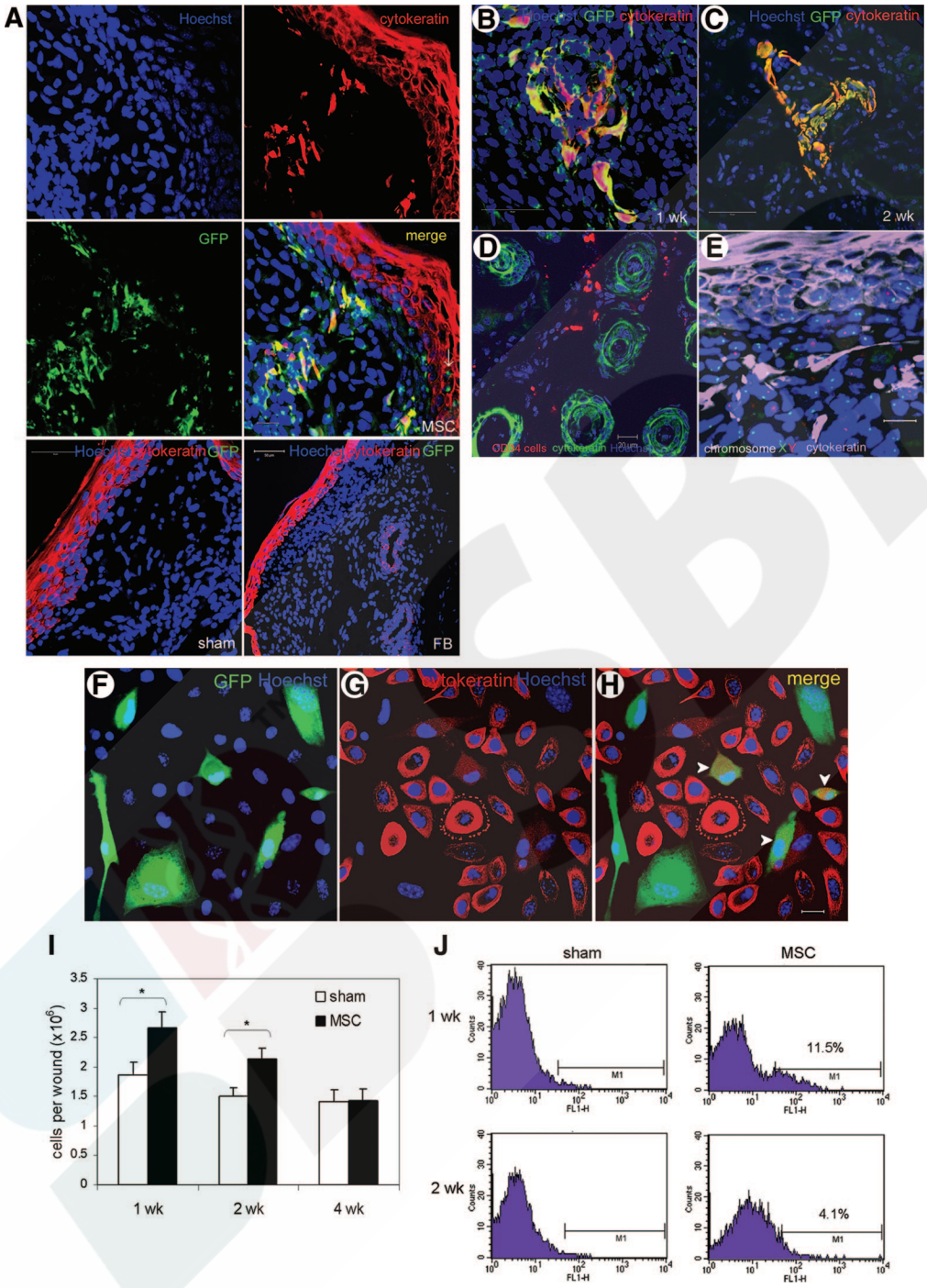

Figure 4. Differentiation and engraftment of bone marrow-derived (BM)-MSCs. Tissue sections were immunostained with an anti-pan-cytokeratin antibody. Nuclei (blue) were stained with Hoechst. **(A):** Confocal microscopy showed that cytokeratin-positive (red) BM-MSCs (green) appeared in the dermis and epidermis (indicated by arrows) of a day 7 BM-MSC-treated wound but not vehicle medium- or FB-treated wound. Scale bar = 50 μm. **(B, C):** GFP$^+$ BM-MSCs (green) expressing cytokeratin (red) formed a nodule that resembled early sweat or sebaceous glands in the dermis of a day 7 wound **(B)**, and such structures became more mature in wounds at 14 days **(C)**. Scale bar = 50 μm. **(D):** Implanted DiI-labeled CD34$^+$ BM cells (red) were shown in a day 10 wound. Keratinocytes were stained green, and nuclei were stained blue. Scale bar = 20 μm. **(E):** A representative image of X and Y chromosome fluorescence in situ hybridization stain of a day 7 MSC-treated wound. Y-chromosome (red)-positive cells derived from implanted MSCs contained no more than one X-chromosome (green). Cytokeratin was immunostained pink. Scale bar = 20 μm. **(F–H):** Confocal microscopic images showing GFP$^+$ BM-MSCs (green) cocultured with preirradiated dermal keratinocytes for 1 wk after immunostaining for cytokeratins (red). Nuclei were stained with Hoechst (blue). After merging **(F)** and **(G)**, cells expressing GFP and cytokeratins are indicated in yellow (arrowhead **[H]**). Scale bar = 20 μm. **(I):** The number of cells per wound was determined after digestion of the entire wound (n = 5; t test, *, $p < .001$). **(J):** One representative result of five fluorescence-activated cell sorting analyses of skin digests for GFP-positive cells at different times after wounding. Cells from sham wounds were used for negative controls and gate setting. Values represent percentages of GFP-positive cells. Abbreviations: FB, fibroblasts; GFP, green fluorescent protein; wk, week(s).

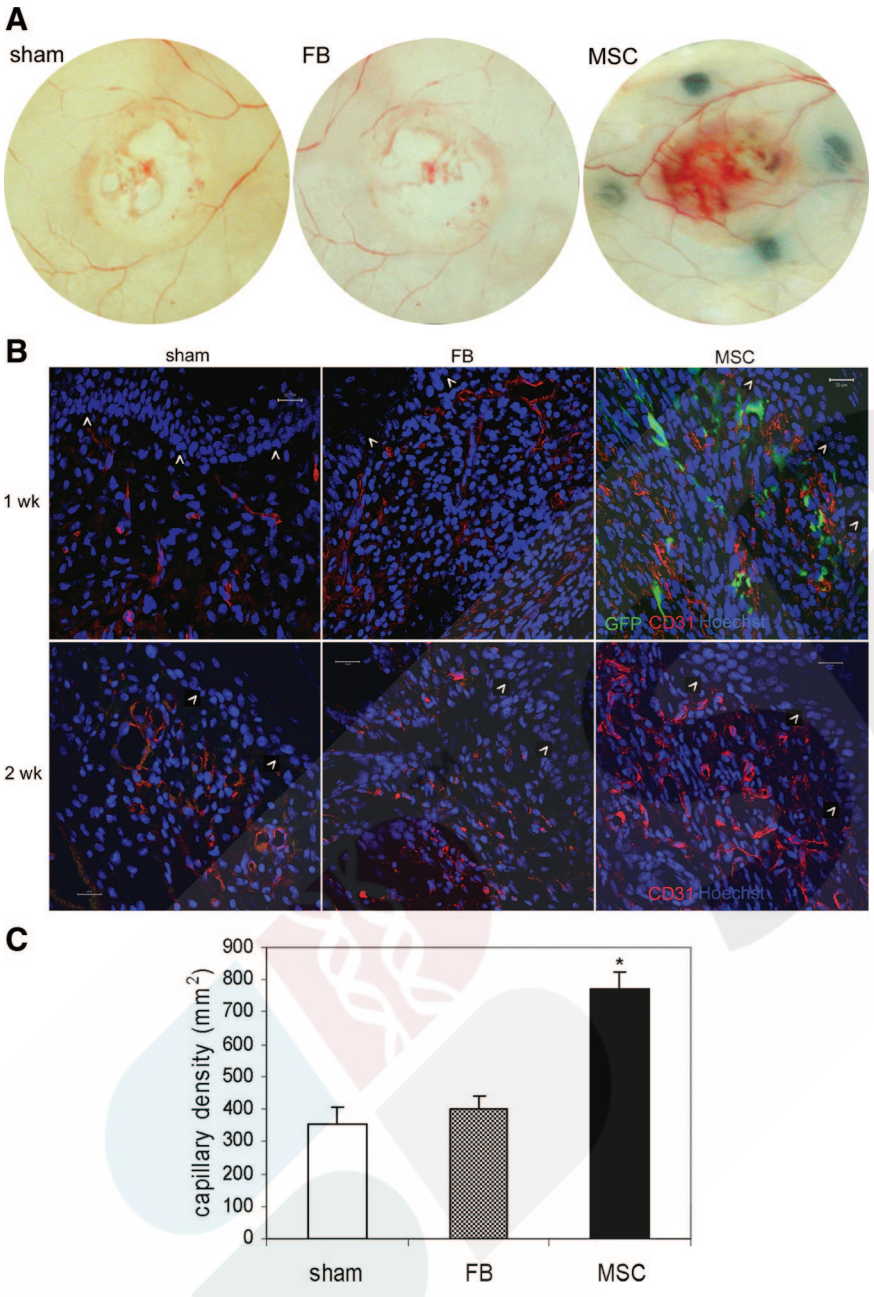

Figure 5. Effects of BM-MSC on wound vascularity. **(A):** Representative images of whole skin mounts of day 7 wounds in BALB/c mice treated with vehicle medium (sham), FB, or MSC. Vehicle- or FB-treated wound appeared more transparent with defects (holes), whereas BM-MSC-treated wound shows blood vessels growing from surrounding tissue. **(B):** Immunofluorescence for endothelial cells. Day 7 (upper panel) or 14 (lower panel) wound sections were stained with an anti-CD31 antibody and detected with Fluor 568 (red). Nuclei were stained with Hoechst. Arrowheads indicate the epidermis. Scale bar = 20 μm. **(C):** Capillary density in 2-wk-old wounds was counted after CD31 staining ($n = 6$; *, $p < .0001$). Abbreviations: FB, fibroblasts; GFP, green fluorescent protein; MSC, bone marrow-derived MSCs; wk, week(s).

enhanced cutaneous regeneration. Indeed, BM-MSC-treated wounds exhibited increased numbers of appendage-like structures at 7 days compared with vehicle medium- or fibroblast-treated wounds (sham, 4.5 ± 0.42; fibroblast, 4.7 ± 0.53; MSC, 10.2 ± 0.79 per wound section; $n = 5$; MSC vs. sham or fibroblast, $p < .001$). We then measured the fractions of dividing cells in the wound sections after staining for Ki67 [27]. As shown in Figure 3D and 3E, BM-MSC-treated wounds exhibited significantly increased proportions of Ki67-positive cells, along with increased numbers of Ki67-positive hair follicle- or sweat/sebaceous gland-like structures (with more than 10% Ki67-positive nuclei) compared with vehicle medium- or fibroblast-treated wounds (Fig. 3E, 3F; $n = 5$; $p < .001$). Fibroblast-treated wounds showed increased numbers of Ki67-positive cells (Fig. 3E; $p < .01$) but not Ki67-positive appendages (Fig. 3F).

BM-MSCs Contribute to Dermal Keratinocytes and Appendages

To determine whether BM-MSCs in the wounded skin could contribute to keratinocytes, we performed immunostaining for GFP and epithelial protein cytokeratin. We used an anti-cytokeratin antibody that reacted to several keratin subunits (K4, K5, K6, K8, K14, and K16). In the day 7 wound, GFP and cytokeratin double-positive cells were found especially in the dermis adjacent to the epidermis, and some appeared in the epidermis (Fig. 4A). Some BM-MSCs positive for GFP and cytokeratin in the dermis of the wounded skin formed structures that resembled developing sweat or sebaceous glands (Fig. 4B). Such structures appeared more mature at 14 days (Fig. 4C). GFP^+ cells were not detected in GFP-negative fibroblast- or vehicle medium-treated wounds (Fig. 4A), indicating specificity of the immunostaining. To determine the fractions of BM-MSCs ex-

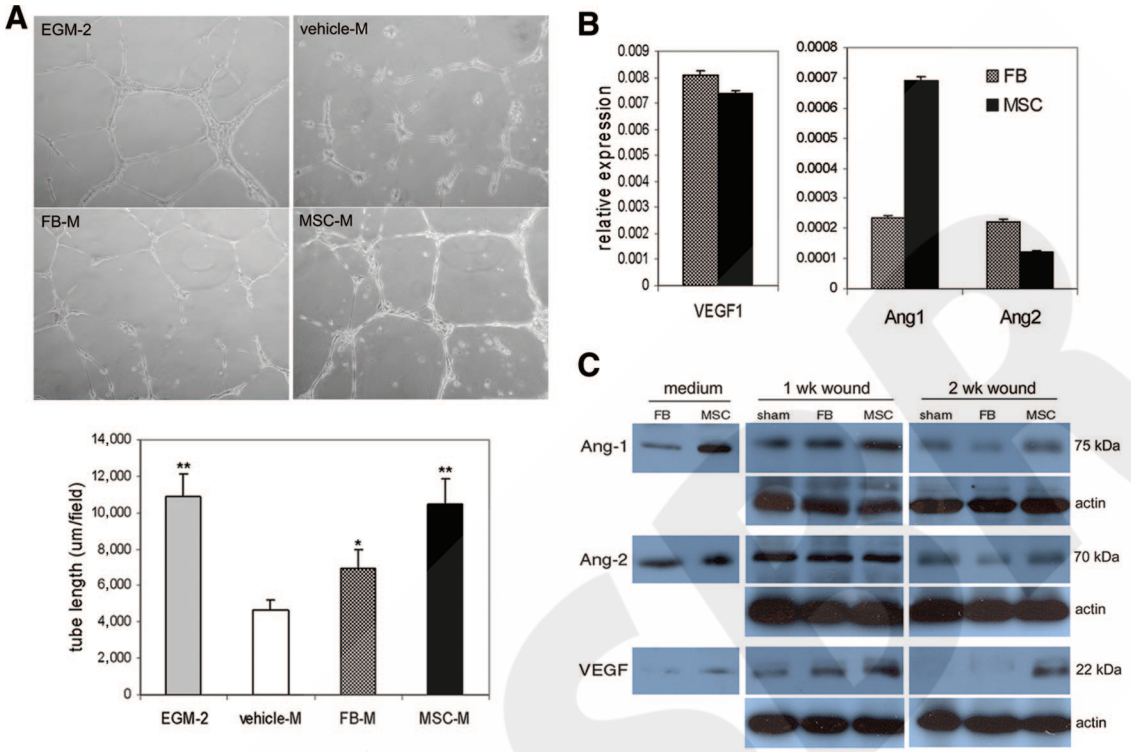

Figure 6. Effects of bone marrow-derived MSC (BM-MSC)-conditioned medium on human umbilical vein endothelial cells (HUVECs). **(A):** Endothelial cell tube formation. HUVECs were suspended in vehicle-, MSC-, or FB-conditioned basal EGM-2 supplemented with 0.75% fetal bovine serum (FBS) or complete EGM-2, which contained growth factor cocktail and 2% FBS, and incubated for 24 hours. Representative fields are shown. The total length of the tube network per field was quantified. Experiments were performed in triplicate wells ($n = 4$; *, $p < .05$; **, $p < .001$). **(B):** Real-time polymerase chain reaction analysis shows expression levels of VEGF-α, Ang-1, and Ang-2 (relative to glyceraldehyde-3-phosphate dehydrogenase) in BM-MSCs and FBs. **(C):** Western blot assay shows expression of VEGF-α, Ang-1, and Ang-2 in FB- or BM-MSC-conditioned medium and vehicle medium (sham)-, FB-, or BM-MSC-treated wounds. The experiment was repeated three times, and one representative result is shown. Abbreviations: Ang, angiopoietin; EGM, epithelial growth medium; FB, fibroblast; FB-M, fibroblast medium; MSC-M, bone marrow-derived MSC medium; VEGF, vascular endothelial growth factor; vehicle-M, vehicle medium; wk, week.

pressing cytokeratin, we analyzed cells derived from digestion of wounds. Slides were prepared on a cytospin and immunostained for GFP and cytokeratin. Analysis of 200 GFP-expressing cells per sample indicated that 15.3% ± 2.1% of them in day 7 wounds ($n = 5$) and 47.6% ± 6.3% of them in day 14 wounds ($n = 5$) were cytokeratin-positive. To determine whether $CD34^+$ cells contribute to keratinocytes, we implanted equal numbers of DiI-labeled $CD34^+$ murine bone marrow cells to excisional wounds in nude mice ($n = 3$) [28]. Immunofluorescence analysis of wound sections at 10 days for cytokeratin expression using an anti-pan-cytokeratin antibody (the same antibody as used in Fig. 4A–4C) showed engraftment of DiI-$CD34^+$ cells, but none of them expressed cytokeratin or were localized with appendages (Fig. 4D). To determine whether the GFP and cytokeratin double-positive cells were derived from cell fusion, we performed X and Y chromosome FISH using FITC-labeled X-chromosome probe and Cy3-labeled Y-chromosome. BM-MSCs were derived from male mice, whereas the recipient mice were female. Cytokeratin was counterstained and detected with a Cy5-labled secondary antibody. Y-chromosome-positive cells were detected in the dermis and epidermis (Fig. 4E). Some Y-chromosome-positive cells were also positive for cytokeratin but contained no more than one X-chromosome, indicating that the cells were not derived from fusion of MSCs with keratinocytes. To examine whether BM-MSCs differentiate into keratinocytes in vitro, we cultured GFP^+ BM-MSCs (negative for cytokeratins) with preirradiated keratinocytes in a medium favoring keratinocyte growth. Seven days later, immunostaining for cytokeratins indicated that 17.2% ± 4.3% of BM-MSCs became cytokeratin-positive (Fig. 4F–4H).

Engraftment of BM-MSCs into the Wounded Skin

Immunostaining of wound sections for GFP showed a large number of GFP^+ BM-MSCs in BM-MSC-treated wounds at 7 days. The cells were mostly found in the newly formed dermis, but some appeared in the epidermis (Fig. 4A). GFP^+ cells were not detected in the surrounding normal skin. Decreased numbers of GFP^+ BM-MSCs were localized to the centers of wounds and skin appendages at 14 days; in addition, markedly fewer GFP^+ BM-MSCs were detected in the wound at 28 days. To determine the numbers of GFP^+ BM-MSCs engrafted into the wounded skin at different stages, we excised the entire wound along with a small amount of the surrounding skin and dispersed it into a single cell suspension. Counting of cells in the suspension with a cytometer resulted in the number of total cells per wound: in the sham group, $1.86 \pm 0.22 \times 10^6$ at 7 days, $1.51 \pm 0.14 \times 10^6$ at 14 days, and $1.42 \pm 0.19 \times 10^6$ at 28 days; in BM-MSC-treated mice, $2.67 \pm 0.27 \times 10^6$ at 7 days, $2.16 \pm 0.18 \times 10^6$ at 14 days, and $1.44 \pm 0.20 \times 10^6$ at 28 days (Fig. 4I). FACS analysis of the skin digests for GFP-positive cells indicated that 10.1% ± 1.7% at 7 days, 3.5% ± 0.48% at 14 days (Fig. 4J; $n = 5$), and 1.8% ± 0.21% at 28 days of the total cells were GFP-positive in BM-MSC-treated wounds. Taking the initially implanted 1 million BM-MSCs per wound as 100%, after calculation, BM-MSC engraftment to the wound was 27% at 7 days, 7.6% at 14 days, and 2.5% at 28 days.

BM-MSCs Enhance Angiogenesis

The BALB/c mouse skin is thin and semitransparent, which allows macroscopic visualization of blood vessels. In wounds of sham and fibroblast groups at 7 days in BALB/c mice, blood vessels were seen clearly in the skin surrounding the wounds but were limited in the wounds. In contrast, in wounds of MSC group, vessels and their fine branches extended into the wounds, forming networks (Fig. 5A). Immunohistological staining of tissue sections for endothelial protein CD31 (Fig. 5B) or vWF (data not shown) showed increased vasculature in BM-MSC-treated wounds at 7 and 14 days compared with vehicle medium- or fibroblast-treated wounds. Capillary densities in wounds at 14 days were assessed morphometrically after immunohistochemical staining for CD31 [21, 22]. As shown in Figure 6C, capillary density was significantly higher in BM-MSC-treated wounds ($771 \pm 55/mm^2$) than in vehicle medium-treated ($357 \pm 51/mm^2$) or fibroblast-treated ($398 \pm 44/mm^2$) wounds ($n = 5$; $p < .001$). BM-MSCs appeared close to vasculature but were not in the walls of blood vessels. To determine whether BM-MSCs could enhance angiogenesis through a paracrine effect, we cultured HUVECs in BM-MSC-conditioned medium derived from culturing of BM-MSCs under hypoxic conditions ($<1\%$ O_2) for 24 hours and found that the medium significantly enhanced HUVEC tube formation on Matrigel compared with vehicle control medium or fibroblast-conditioned medium (Fig. 6A). Real-time PCR analysis showed that VEGF-α was highly expressed in BM-MSCs and fibroblasts, but the Ang-1/Ang-2 ratio was much greater in BM-MSCs (5.7) than in fibroblasts (1.07) (Fig. 6B). To examine the protein expression levels of these genes, we performed Western blot analysis of concentrated BM-MSC- or fibroblast-conditioned medium under hypoxic conditions and lysate derived from vehicle medium (sham)-, fibroblast- or BM-MSC-treated wounds. Our data showed a greater amount of Ang-1 protein in BM-MSC-conditioned medium and higher levels of Ang-1 in BM-MSC-treated wounds at 7 and 14 days but unchanged amounts of Ang-2 (Fig. 6C). Under reducing conditions, the anti-VEGF-α antibody detected a major band of approximately 22 kDa, which corresponds to the molecular size of VEGF164 [29]. Of note, larger amounts of VEGF-α were detected in BM-MSC-treated wounds compared with vehicle medium- or fibroblast-treated wounds at 7 and 14 days (Fig. 6C).

DISCUSSION

Diabetic ulcers and other chronic wounds are difficult to heal, and little improvement has been shown in preventing the associated morbidity and disability in the past few decades [4]. The best available treatment for chronic wounds achieves only a 50% healing rate that is often temporary. Innovative treatments to enhance wound healing and regeneration are needed. Here, we show that BM-MSCs enhance wound healing in nondiabetic and diabetic mice by promoting re-epithelialization, cell infiltration, and angiogenesis.

We used an excisional wound splinting model and found that splinting prevented skin contraction and allowed wounds to heal through granulation and re-epithelialization, as reported previously [18]. In addition, the model resulted in uniform wound closure due to minimization of variations caused by skin contraction and wound dressings. To assess the effect of BM-MSCs in healing diabetic wounds, we used genetically diabetic *db/db* mice, which have been known to have markedly impaired wound healing and have been used extensively to study the effect of therapeutic reagents on wound healing [19, 20]. Indeed, our *db/db* mice exhibited significant obesity, hyperglycemia, and hyperlipidemia, symptoms similar to type II diabetes. Our results indicate that wound closure is significantly delayed in the mice and implantation of BM-MSCs significantly promotes the wound healing process. Consistent with our findings, BM-MSCs was recently shown to increase the tensile strength of incisional wounds in nondiabetic rats [30].

We have shown that a substantial fraction of GFP-expressing BM-MSCs engrafted in the wound appeared to coexpress cytokeratin subunits and therefore may adopt an epithelial-like phenotype. Moreover, some GFP-expressing BM-MSCs were found to form sweat or sebaceous gland-like structures. Our finding is consistent with a recent study in which intravenously infused 5-bromo-2′-deoxyuridine-labeled ex vivo-expanded bone marrow adherent cells containing MSCs and $CD34^+$ cells were found to contribute to cells in hair follicles, sebaceous glands, and blood vessels in the dermis of full-thickness skin wounds [31]. Notably, in our study, similarly implanted $CD34^+$ bone marrow cells did not express cytokeratin or incorporate into skin epidermis and appendages in the wound. Our results indicate that BM-MSCs but not $CD34^+$ cells can contribute to cutaneous structures. In a previous study, BM-MSCs were found to repair epithelium in vitro through differentiation and fusion [32]. Our X and Y chromosome FISH data suggest that the cytokeratin-expressing MSCs in the wound are formed via differentiation but not cell fusion. In a recent study, similarly transplanted ex vivo-expanded BM-MSCs were found to differentiate into hepatocytes without evidence of cell fusion [6]. In postpartum humans, injury to the skin and other tissues heals not by the regeneration of the tissue to the preinjured form but by the formation of scar tissue. Our data and those of others suggest that BM-MSCs engrafted in the wound may contribute to cells in the skin epidermis and appendages, thus mediating dermal regeneration. Of note, our data showed limited GFP-expressing epithelial cells in the wound by 4 weeks when the wound was closed. This is probably due to rapid turnover of epithelial cells during wound healing. Consistent with our findings, epithelial cells derived from endogenous bone marrow cells were found transiently during wound healing [23]. These data suggest that the bone marrow may not provide long-term self-renewal stem cells for dermal keratinocytes. In this study, we found that BM-MSC-treated wounds exhibited a significantly increased number of regenerating appendage-like structures rich in Ki67-positive dividing cells. Interestingly, these structures were largely formed by endogenous keratinocytes, suggesting that paracrine factors released by engrafted BM-MSCs in the wound also play an important role in cutaneous regeneration.

We determined the numbers of GFP-positive BM-MSCs in the wound at various stages of wound healing by FACS analysis coupled with immunohistochemical assessment. Our data indicate a substantial engraftment of BM-MSCs in the day 7 wounds and a rapid reduction of the cells in the day 14 wounds and thereafter. Consistent with our findings, a recent study showed a dramatic decline of engrafted BM-MSCs in the acutely infarcted myocardium after intramyocardial injection [33]. The mechanisms involved with the decline of implanted MSCs are not fully understood. It is likely that with progression of wound healing process, cytokines and ECM molecules favorable to MSC survival and engraftment decrease. It is known that engraftment of BM-MSCs to normal nonhematopoietic tissues is extremely low.

Neovascularization is a crucial step in the wound healing process [1–3, 34]. The formation of new blood vessels is necessary to sustain the newly formed granulation tissue and the survival of keratinocytes. In this study, we demonstrated that BM-MSC-treated wounds had enhanced capillary density, suggesting that BM-MSCs promote angiogenesis; however, BM-MSCs were not found in the vascular structures but in close

proximity. The discrepancy led us to study the paracrine effect of BM-MSCs in angiogenesis. Indeed, we found that BM-MSC-conditioned medium promoted endothelial tube formation and that BM-MSCs expressed high levels of VEGF-α and Ang-1 but not Ang-2. Notably, BM-MSC treatment resulted in significantly increased amounts of Ang-1 and VEGF-α in the wounds. VEGF plays a key role in angiogenesis by stimulating endothelial cell proliferation, migration, and organization into tubules [34, 35]. Moreover, VEGF increases circulating endothelial progenitor cells [35]. The angiopoietins represent another major family of angiogenic factors. Ang-1 and Ang-2 are ligands for the Tie2 receptor tyrosine kinase that is present on endothelial cells and endothelial progenitor cells. Ang-1-Tie2 interactions mediate neovessel maturation into more complex and larger vascular structures and maintain vessel integrity through the recruitment of periendothelial cells and the reestablishment of basement membrane. Ang-2, as an endogenous antagonist of Tie2, functions to block this Ang1-Tie2 signaling [34, 35]. Angiogenesis is a complex process controlled by the balance of proangiogenic and antiangiogenic factors [35]. Our results suggest that BM-MSCs engrafted in the wound release proangiogenic factors, which may be partially responsible for MSC-mediated enhanced angiogenesis.

Low incidence of differentiation of MSCs into cardiomyocytes was reported recently [33], and procrine mechanism was suggested to play a major role in MSC-mediated myocardial repair [36, 37]. However, the incidences of differentiation of MSCs into keratinocytes found in this study and others are much higher [38, 39]. In our recent study, we found that injection of MSC-conditioned medium could accelerate wound closure, but the enhancement was less dramatic and the wound quality was less evidently improved compared with cell implantation (data not shown). Theses results suggest that differentiation of MSCs may be indispensable in MSC-mediated cutaneous repair/regeneration, although paracrine factors are important.

In this study, we used purified BM-MSCs, which eliminated blood lineage cells, aiming to verify the bone marrow cells accounting for cutaneous regeneration and enhanced wound healing. Previous studies suggest that other populations of BM cells may also be beneficial to the healing of chronic wounds. Freshly isolated BM cells enriched for hematopoietic progenitor cells from nondiabetic mice were found to promote wound healing in diabetic *db/db* mice, but impaired functions were found with the cells derived from *db/db* mice [40]. Application of macrophages derived from healthy donors was found to promote healing of chronic ulcers in patients [41].

Our results did not show enhancement of wound healing in allogeneic fibroblast-treated nondiabetic mice, although modest improvement was observed in the early stages in *db/db* mice. Previously, patients with diabetic or venous skin ulcers have been treated with two FDA-approved engineered living skin products containing allogeneic fibroblasts [42]; however, the benefit of allogeneic fibroblasts in wound healing remains controversial [43, 44]. Our study showed a lower number of allogeneic fibroblasts engrafted into the wound compared with allogeneic BM-MSCs. In a previous study, allogeneic fibroblasts was found to cause increased inflammation and scar formation [44].

In conclusion, this study demonstrates systemically the beneficial effect of BM-MSCs in cutaneous regeneration and wound healing in nondiabetic and diabetic mice through differentiation and paracrine effects. Administration of allogeneic BM-MSCs or BM-MSC-derived molecules may represent novel therapeutic approaches in the treatment of chronic wounds and other conditions.

ACKNOWLEDGMENTS

We gratefully acknowledge H.A. Shankowsky for excellent assistance with animal protocols and secretary and M. Cao for technical support. This work was supported in part by Firefighters' Burn Trust Fund and the University of Alberta Hospital Foundation.

DISCLOSURE OF POTENTIAL CONFLICTS OF INTEREST

The authors indicate no potential conflicts of interest.

REFERENCES

1 Martin P. Wound healing—Aiming for perfect skin regeneration. Science 1997;276:75–81.
2 Falanga V. Wound healing and its impairment in the diabetic foot. Lancet 2005;366:1736–1743.
3 Singer AJ, Clark RA. Cutaneous wound healing. N Engl J Med 1999; 341:738–746.
4 Boulton AJ, Vileikyte L, Ragnarson-Tennvall G et al. The global burden of diabetic foot disease. Lancet 2005;366:1719–1724.
5 Pittenger MF, Mackay AM, Beck SC et al. Multilineage potential of adult human mesenchymal stem cells. Science 1999;284:143–147.
6 Sato Y, Araki H, Kato J et al. Human mesenchymal stem cells xenografted directly to rat liver are differentiated into human hepatocytes without fusion. Blood 2005;106:756–763.
7 Toma C, Pittenger MF, Cahill KS et al. Human mesenchymal stem cells differentiate to a cardiomyocyte phenotype in the adult murine heart. Circulation 2002;105:93–98.
8 Kopen GC, Prockop DJ, Phinney DG. Marrow stromal cells migrate throughout forebrain and cerebellum, and they differentiate into astrocytes after injection into neonatal mouse brains. Proc Natl Acad Sci U S A 1999;96:10711–10716.
9 Kondo T, Johnson SA, Yoder MC et al. Sonic hedgehog and retinoic acid synergistically promote sensory fate specification from bone marrow-derived pluripotent stem cells. Proc Natl Acad Sci U S A 2005;102: 4789–4794.
10 Amado LC, Saliaris AP, Schuleri KH et al. Cardiac repair with intramyocardial injection of allogeneic mesenchymal stem cells after myocardial infarction. Proc Natl Acad Sci U S A 2005;102:11474–11479.
11 Jin HK, Carter JE, Huntley GW et al. Intracerebral transplantation of mesenchymal stem cells into acid sphingomyelinase-deficient mice delays the onset of neurological abnormalities and extends their life span. J Clin Invest 2002;109:1183–1191.
12 Li Y, Chen J, Zhang CL et al. Gliosis and brain remodeling after treatment of stroke in rats with marrow stromal cells. Glia 2005;49:407–417.
13 Keating A. Mesenchymal stromal cells. Curr Opin Hematol 2006;13: 419–425.
14 Colter DC, Class R, DiGirolamo CM et al. Rapid expansion of recycling stem cells in cultures of plastic-adherent cells from human bone marrow. Proc Natl Acad Sci U S A 2000;97:3213–3218.
15 Fathke C, Wilson L, Hutter J et al. Contribution of bone marrow-derived cells to skin: Collagen deposition and wound repair. STEM CELLS 2004;22:812–822.
16 Tropel P, Noel D, Platet N et al. Isolation and characterisation of mesenchymal stem cells from adult mouse bone marrow. Exp Cell Res 2004;295:395–406.
17 Baghdoyan S, Lamartine J, Castel D et al. Id2 reverses cell cycle arrest induced by gamma-irradiation in human HaCaT keratinocytes. J Biol Chem 2005;280:15836–15841.
18 Galiano RD, Michaels V, Dobryansky M et al. Quantitative and reproducible murine model of excisional wound healing. Wound Repair Regen 2004;12:485–492.
19 Jacobi J, Jang JJ, Sundram U et al. Nicotine accelerates angiogenesis and wound healing in genetically diabetic mice. Am J Pathol 2002;161:97–104.
20 Galeano M, Altavilla D, Cucinotta D et al. Recombinant human erythropoietin stimulates angiogenesis and wound healing in the genetically diabetic mouse. Diabetes 2004;53:2509–2517.

21 Yoon YS, Murayama T, Gravereaux E et al. VEGF-C gene therapy augments postnatal lymphangiogenesis and ameliorates secondary lymphedema. J Clin Invest 2003;111:717–725.
22 Hamano Y, Zeisberg M, Sugimoto H et al. Physiological levels of tumstatin, a fragment of collagen IV alpha3 chain, are generated by MMP-9 proteolysis and suppress angiogenesis via alphaVbeta3 integrin. Cancer Cell 2003;3:589–601.
23 Borue X, Lee S, Grove J et al. Bone marrow-derived cells contribute to epithelial engraftment during wound healing. Am J Pathol 2004;165: 1767–1772.
24 Fukushi Ji, Makagiansar IT, Stallcup WB. NG2 proteoglycan promotes endothelial cell motility and angiogenesis via engagement of galectin-3 and alpha3beta1 integrin. Mol Biol Cell 2004;15:3580–3590.
25 Miller GE, Chen E. Life stress and diminished expression of genes encoding glucocorticoid receptor and β2-adrenergic receptor in children with asthma. Proc Natl Acad Sci U S A 2006;103:5496–5501.
26 Wu Y, Chen L, Zheng PS et al. β1-Integrin-mediated glioma cell adhesion and free radical-induced apoptosis are regulated by binding to a C-terminal domain of PG-M/versican. J Biol Chem 2002;277:12294–12301.
27 Du Z, Podsypanina K, Huang S et al. Introduction of oncogenes into mammary glands in vivo with an avian retroviral vector initiates and promotes carcinogenesis in mouse models. Proc Natl Acad Sci U S A 2006;103:17396–17401.
28 Wu Y, Ip JE, Huang J et al. Essential role of ICAM-1/CD18 in mediating EPC recruitment, angiogenesis, and repair to the infarcted myocardium. Circ Res 2006;99:315–322.
29 Grutzkau A, Kruger-Krasagakes S, Baumeister H et al. Synthesis, storage, and release of vascular endothelial growth factor/vascular permeability factor (VEGF/VPF) by human mast cells: Implications for the biological significance of VEGF206. Mol Biol Cell 1998;9:875–884.
30 McFarlin K, Gao X, Liu YB et al. Bone marrow-derived mesenchymal stromal cells accelerate wound healing in the rat. Wound Repair Regen 2006;14:471–478.
31 Li H, Fu X, Ouyang Y et al. Adult bone-marrow-derived mesenchymal stem cells contribute to wound healing of skin appendages. Cell Tissue Res 2006;326:725–736.
32 Spees JL, Olson SD, Ylostalo J et al. Differentiation, cell fusion, and nuclear fusion during ex vivo repair of epithelium by human adult stem cells from bone marrow stroma. Proc Natl Acad Sci U S A 2003;100: 2397–2402.
33 Noiseux N, Gnecchi M, Lopez-Ilasaca M et al. Mesenchymal stem cells overexpressing Akt dramatically repair infarcted myocardium and improve cardiac function despite infrequent cellular fusion or differentiation. Mol Ther 2006;14:840–850.
34 Arnold F, West DC. Angiogenesis in wound healing. Pharmacol Ther 1991;52:407–422.
35 Fam NP, Verma S, Kutryk M et al. Clinician guide to angiogenesis. Circulation 2003;108:2613–2618.
36 Kinnaird T, Stabile E, Burnett MS et al. Local delivery of marrow-derived stromal cells augments collateral perfusion through paracrine mechanisms. Circulation 2004;109:1543–1549.
37 Gnecchi M, He H, Liang OD et al. Paracrine action accounts for marked protection of ischemic heart by Akt-modified mesenchymal stem cells. Nat Med 2005;11:367–368.
38 Wang G, Bunnell BA, Painter RG et al. Adult stem cells from bone marrow stroma differentiate into airway epithelial cells: Potential therapy for cystic fibrosis. Proc Natl Acad Sci U S A 2005;102:186–191.
39 Medina RJ, Kataoka K, Miyazaki M et al. Efficient differentiation into skin cells of bone marrow cells recovered in a pellet after density gradient fractionation. Int J Mol Med 2006;17:721–727.
40 Stepanovic V, Awad O, Jiao C et al. Leprdb diabetic mouse bone marrow cells inhibit skin wound vascularization but promote wound healing. Circ Res 2003;92:1247–1253.
41 Zuloff-Shani A, Kachel E, Frenkel O et al. Macrophage suspensions prepared from a blood unit for treatment of refractory human ulcers. Transfus Apher Sci 2004;30:163–167.
42 Griffith LG, Naughton G. Tissue engineering—Current challenges and expanding opportunities. Science 2002;295:1009–1014.
43 Hasegawa T, Suga Y, Mizoguchi M et al. An allogeneic cultured dermal substitute suitable for treating intractable skin ulcers and large skin defects prior to autologous skin grafting: Three case reports. J Dermatol 2005;32:715–720.
44 Lamme EN, Van Leeuwen RTJ, Mekkes JR et al. Allogeneic fibroblasts in dermal substitutes induce inflammation and scar formation. Wound Repair Regen 2002;10:152–160.